Multiclass change detection for multidimensional images in the presence of noise

Javier López-Fandiño, Dora B. Heras, Francisco Argüello

Javier López-Fandiño, Dora B. Heras, Francisco Argüello, "Multiclass change detection for multidimensional images in the presence of noise," Proc. SPIE 10792, High-Performance Computing in Geoscience and Remote Sensing VIII, 1079204 (9 October 2018); doi: 10.1117/12.2325363

SPIE.

Event: SPIE Remote Sensing, 2018, Berlin, Germany

Multiclass Change Detection for Multidimensional Images in the Presence of Noise

Javier López-Fandiño[a], Dora B. Heras[a], and Francisco Argüello[b]

[a]Centro Singular de Investigación en Tecnoloxías da Información (CiTIUS), Universidade de Santiago de Compostela, Santiago de Compostela, Spain
[b]Departamento de Electrónica e Computación, Universidade de Santiago de Compostela, Santiago de Compostela, Spain

ABSTRACT

Change Detection (CD) techniques applied over multitemporal multispectral or hyperspectral remote sensing images allow monitoring changes in the land use or catastrophe tracking, among other applications. A multiclass CD technique for multidimensional images that is robust in the presence of noise is presented in this paper. The technique combines fusion at feature level to perform a first change/no change labeling (binary CD) and a later stage with fusion at decision level that performs a supervised multidate classification of the changed pixels (multiclass CD) obtaining the final *from-to* change map. The acquisition of multidimensional images usually corrupts the original signal by adding noise. This noise can be related with natural random processes or it can be produced during the sensor operation. Additive White Gaussian Noise (AWGN) and speckle noise simulate these effects. In this paper the robustness of the proposed CD technique in noisy scenarios for these two types of noise of varying intensity is evaluated. The experimental results show that the proposed technique is more robust than other alternatives, achieving accuracies close to those obtained in the absence of noise. The proposed technique is designed to be efficiently computed in GPU, thus dealing with the high computational cost of the processing of multidimensional images.

Keywords: Multiclass change detection, remote sensing, noise, classification, GPU.

1. INTRODUCTION

Multidimensional remote sensing imagery comprises several spectral bands encompassing different contiguous wavelengths that provide exhaustive information on the captured scene. The availability of multitemporal multidimensional datasets, including the same scene captured at different time-frames, make it possible to apply Change Detection (CD) techniques with the aim of identifying those regions of the scene that have changed across time. Different applications require to know different types and sizes of changes. These techniques can tackle problems regarding the evolution of land use, precision agriculture, urban growth analysis, deforestation rate calculation, or catastrophe tracking, among others.[1]

CD is a key process in the field of remote sensing as it provides useful information corresponding to processes over the Earth surface. This way CD techniques are eligible to complement or even substitute in-situ inspection. CD techniques can be grouped depending on whether the multitemporal data is merged at the feature or at the decision level.[2] In the first approach, both images are combined prior to performing the CD. This approximation usually relies on the use of algebra operations on both images, such as image differencing or image ratioing, vegetation index differencing,[3] or any technique based on Change Vector Analysis (CVA)[4] such as compressed change vector analysis.[5,6] CVA-based techniques are a group of techniques that rely on the computation of distances and angles between pairs of pixels corresponding to the same position in both images. Other techniques where the fusion is performed at feature level are based on fuzzy methods, assuming some overlap between the change and no change classes. Context based approaches such as Markov Random Fields (MRF)[7] or Expectation-Maximization-based Level Set (EMLS)[8] are the base for other methods.

Further author information: E-mail: {javier.lopez.fandino, dora.blanco, francisco.arguello}@usc.es

High-Performance Computing in Geoscience and Remote Sensing VIII, edited by Bormin Huang, Sebastián López, Zhensen Wu, Proc. of SPIE Vol. 10792, 1079204 · © 2018 SPIE
CCC code: 0277-786X/18/$18 · doi: 10.1117/12.2325363

In the case of methods where the fusion of the multitemporal data is achieved at the decision level, a direct multidate classification, considering all the multitemporal information together, is the solution applied in some cases,[9] while other methods compute the classification of the two images separately and compare the classification maps obtained.[10]

Dimensionality reduction techniques have been investigated and extensively used in multidimensional remote sensing analysis. These techniques allow reducing the dimensionality of the data by applying linear or non-linear transformations. In the context of CD an adequate Feature Extraction (FE) technique[11] allows us reducing the dimensionality of the original data while enhancing the features associated to changes in the multitemporal image. Principal Component Analysis (PCA)[12] or Non-parametric Weighted Feature Extraction (NWFE)[13] are suitable options to perform this process in multidimensional remote sensing datasets.

The multidimensional image acquisition process usually results in the addition of noise to the original signal.[14] This noise can be introduced by different factors, such as natural random processes or due to the sensor operation itself. The presence of noise in the spectra signatures captured by remote sensing sensors is common. This effect can be especially harmful in CD scenarios because the noise in the images to be processed for CD can result in the detection of false changes. Additive White Gaussian Noise (AWGN) and speckle noise[15] are used in this paper to simulate these effects in the experiments, and measure the robustness of the proposed CD technique in these scenarios.

Remote sensing applications are computationally demanding, therefore, they are good candidates to be projected onto High Performance Computing (HPC) infrastructures such as clusters or specialized hardware devices.[16,17] In the past, some remote sensing applications have been executed in Field Programmable Gate Arrays (FPGA)[18,19] or Graphics Processing Units (GPUs)[16,20–22] with the aim of improving their execution times. Commodity GPUs provide a cost-efficient solution to perform on-board real-time processing of remote sensing data.[23] introduces a nearest neighbor hierarchical CD framework for crop monitoring where only the most computationally expensive step is executed in GPU.[24] presents a CD technique based on image differencing and fuzzy clustering on AMD GPUs.

In this paper, a multiclass CD technique based on FE and direct multidate classification is proposed. The technique is designed to be efficiently computed in GPU and its robustness in noisy scenarios is validated. First, a binary CD stage with fusion at the feature level is introduced, with the aim of filtering the pixels corresponding to the no change class. The multitemporal data is merged and the relevant change features are extracted. Only pixels that have passed the binary filtering are considered in the final classification stage.

2. MULTICLASS CD TECHNIQUE FOR MULTIDIMENSIONAL IMAGES

The technique proposed in this paper for CD applied to multidimensional images is shown in Fig. 1. The technique includes both binary and multiclass stages, that are merged through a filtering stage before performing the final CD classification stage. The following paragraphs are devoted to the introduction of all the stages involved in the proposed CD technique.

The binary stage of the CD scheme (top stage on Fig. 1) was introduced in detail in a previous paper.[25] Its objective is to label each pixel as change or no change to obtain a mask to be used in a later filtering stage.

As shown in Fig. 1, the binary CD stage is computed as the difference of the two segmented images, followed by a thresholding that discriminates between change and no change pixels. The difference between the images is calculated at pixel level by using the Spectral Angle Mapper (SAM) distance:

$$\alpha_{i,j} = \frac{2}{\pi} \cos^{-1}\left(\frac{S_j \cdot S_i}{\|S_j\|\|S_i\|}\right) \in [0,1], \tag{1}$$

where i and j are the two pixels under consideration and $\alpha_{i,j}$ is the spectral angle between the spectrum of pixel i (S_i) and pixel j (S_j).

A thresholding is then applied to the difference image, by means of Otsu's algorithm, to obtain a binary change detection map. It requires to calculate a histogram of the difference image. This histogram is created with as many bins as the maximum difference value in the image to keep as much information as possible. Otsu's

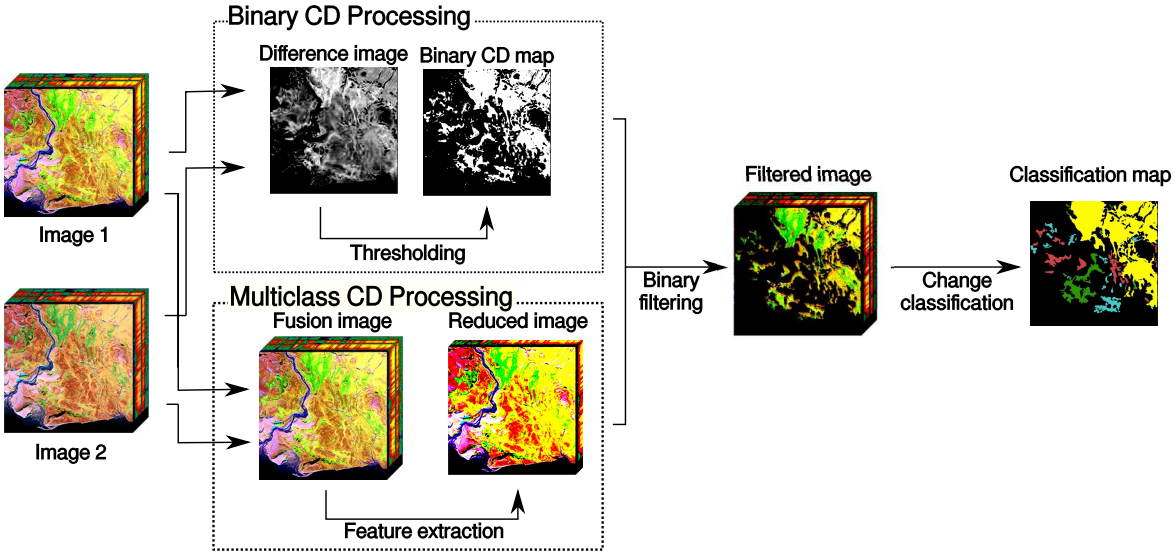

Figure 1: Multiclass CD technique flow-chart.

algorithm considers two classes of pixels in the histogram. The optimal threshold is iteratively computed as the one that provides the minimum intra-class variance, defined as the weighted sum of variances of the two classes:

$$\sigma_w^2(t) = w_0(t)\sigma_0^2(t) + w_1(t)\sigma_1^2(t), \tag{2}$$

being σ_0^2 and σ_1^2 the variances of two classes whose probabilities, separated by a threshold t, are w_0 and w_1. After this, the difference image is processed so that those pixels whose difference value is larger than the threshold are labeled as changed pixels.

Regarding the multiclass stage of the CD scheme (bottom part of Fig. 1), it consists on a change feature processing followed by a direct multidate classification. First, the multitemporal information of the two input images is combined through the fusion of the two images. This fusion can be performed in different ways. The simplest options are to calculate the point by point difference between the input images or stacking all the multitemporal information in a single image. The stack option also allows performing CD in datasets whose images do not share the same spectral size.

Once the multitemporal information is combined in a single image, a FE technique is computed to extract the relevant features of the resulting image, reducing its dimensionality. FE can be addressed by means different techniques,[26] for instance, PCA,[12] NWFE,[13] or by using a Stacked Autoencoder (SAE).[27] PCA and NWFE are the FE methods evaluated in this paper.

Once the multitemporal information is merged and the relevant features extracted, the resulting image is filtered by using the binary CD map that was previously calculated. All the pixels that were considered as no change in the binary CD map are removed from the image. This filtering provides advantages both in the learning of the later classifier, avoiding the learning of the no change class, that is the one with a larger variance in its characteristics, and in terms of computational efficiency, because the number of pixels to classify is smaller. Finally, a supervised classification by Extreme Learning Machine (ELM) or, alternatively, Support Vector Machine (SVM) is performed to obtain the change classification map.

3. GPU COMPUTATION OF THE MULTICLASS CD TECHNIQUE

GPUs provide massively parallel processing capabilities thanks to their data parallel architecture. In particular, for the case of NVIDIA GPUs, the CUDA platform allows us to execute programs invoking parallel kernels that simultaneously execute in many parallel threads following a *single instruction multiple data* programming model.[28] These threads are organized onto blocks forming a grid that is mapped to a hierarchy of CUDA cores

in the GPU. Multiple memory spaces are available to be used for these threads: Private local memory, registers, a shared memory per block whose lifetime equals that of the block, and a global memory that is shared among all threads and is persistent across kernel launches. The NVIDIA PASCAL GPU architecture used in this paper[28] also provides a two level cache hierarchy including a configurable L1 cache for each streaming multiprocessor (SM) and a unified L2 cache shared among all SMs. The architecture provides 96 KB of shared memory for each SM with a block limit of 48 KB.

In order to improve performance, some optimizations have been considered during GPU projection with the objective of fully exploiting the architecture:

1. **Minimize the use of global memory and the number of data transfers between host and device memories.** The use of the global memory is minimized using in-place computation whenever possible, i.e., using the memory reserved for the inputs to store the outputs. All the computations are carried out in the GPU memory so that data transfers between host (CPU) and device (GPU) are reduced to copying the inputs and returning the outputs. It is also essential to minimize the data transfers between global and shared memory.
2. **Search for the best kernel configuration.** The block size is tuned for each kernel to minimize the execution time. The factors involved in the block size selection are the number of registers and the shared memory used by the program. Given that each SM can have a maximum number of active blocks, larger blocks are preferable. The selected block size is a multiple of 32 (the warp size) to avoid divergences among threads an thus maximize parallelism. Additionally, if a computation involves steps requiring different numbers of threads, it is split into consecutive kernels allowing the optimization of the resources and, therefore, maximizing efficiency.
3. **Avoid writing collisions.** When several threads in a kernel need to atomically write in the same structure, it is more efficient to perform independent partial results per block and combine these results in a second kernel.
4. **Efficient use of libraries for common operations.** The cuBLAS,[29] MAGMA,[30] and CULA[31] libraries are used to efficiently compute algebraic operations in GPU.

4. EXPERIMENTS

This section is devoted to the analysis of the CD results achieved with the CD technique proposed in this paper for multidimensional images. First, the experimental setup will be introduced in Section 4.1. Then, Section 4.2 will display the accuracy results as well as the execution times and speedups achieved by running the proposed technique in GPU. Finally Section 4.3 will display the accuracy results obtained in the same dataset considering the inclusion of noise.

4.1 Experimental Setup

The experiments presented in this paper were carried out in the Sardinia dataset displayed in Fig. 2. The Sardinia dataset was acquired by the Thematic Mapper sensor mounted on the Landsat-5 satellite.[32] This dataset was kindly provided by Sicong Liu from the University of Trento and it was used for the evaluation of multitemporal CD methods in several papers from the literature.[6,33,34] It covers a region of the Sardinia Island in Italy, including Lake Mulargia (N 39°37'39.6", E 9°14'13.4"). Two images corresponding to the years 1995 and 1996 are available. The dimensions of the images are 300 × 412 pixels × 6 bands. The spatial resolution is 30 meters per pixel. Fig. 2 (a) and (b) show the color representations of the dataset for the images corresponding to the years 1995 and 1996, respectively, while Fig. 2 (c) displays the reference data of changes available. Three types of changes are considered: an enlargement of an open quarry between the two stages of the lake, a simulated burned area and the enlargement of the lake surface due to the increase of the water volume of the Lake Mulargia. The magnitude of these changes in number of pixels is detailed in Table 1.

A quantitative evaluation of the achieved accuracies was made comparing the achieved change classification maps to the reference data available. Different metrics were used to perform this evaluation:

(a) (b) (c)

Figure 2: Sardinia dataset. Color composition of the input images for the years 1995 (a) and 1996 (b), reference data of changes (c).

Table 1: Classes and distribution of samples for the Sardinia dataset as described in.[6]

Class	Name	Number of samples
1	Enlargement of the quarry	214
2	Simulated burned area	2414
3	Increase of the lake surface	7480
Total		10180

- *The Overall Accuracy (OA)*, that represents the total percentage of correctly classified pixels.
- *The Average Accuracy (AA)*, representing the average percentage of correctly classified pixels for each class. It is the mean of all the class-specific accuracies.
- *The Kappa coefficient (k)*, defined as the percentage of agreement corrected by the amount of agreement that could by expected purely by chance.

Regarding the results of the binary CD stage, where the result obtained is a binary change detection map where each pixel can be assigned to only two different labels: *change* or *no change*.[35] The quality of these maps is evaluated through the use of four different metrics.

- *Correctly classified pixels*, the total number of pixels that were correctly labeled. It can be displayed both in absolute terms and as a percentage of the total amount of pixels in the image.
- *Missed Alarms (MAs)*, i.e., the number of pixels that should have been labeled as change but were labeled as no change. It is expressed in absolute terms.
- *False Alarms (FAs)*, the number of pixels that were incorrectly labeled as change. It is delivered as an absolute value.
- *Total error*, defined as the sum of missed alarms and false alarms. It can be expressed as an absolute value or as a percentage of the total number of pixels in the image.

Finally, the CD technique is also evaluated in terms of time efficiency. This is achieved through the measurement of the execution time. The execution times achieved by the GPU implementations are also compared against optimized multi-threaded OpenMP implementations obtaining a speedup measure (the number of times than the optimized version is faster than the baseline). The execution times detailed in this paper represent the average elapsed time between the start and the end of the computation for 10 independent executions of the code.

Table 2: Binary CD accuracy results for the Sardinia dataset (Correctly classified pixels, MAs, FAs, and total error), in terms of number of pixels and percentage.

Method	Correct		MAs	FAs	Total Error	
C^2VA	117990	(95.46%)	2583	3027	5610	(4.54%)
Euclidean+Otsu	118002	(95.48%)	2586	3012	5598	(4.53%)
SAM+Otsu	**121387**	**(98.21%)**	**1062**	1151	**2213**	**(1.79%)**
Euclidean+watershed+Otsu	117055	(94.70%)	2763	3782	6545	(5.30%)
SAM+watershed+Otsu	121292	(98.13%)	1087	1221	2308	(1.87%)

Table 3: Binary filtering details for the Sardinia dataset (binary CD with SAM+Otsu configuration).

Class	Number of pixels		Filtered pixels		MAs	% of total MAs	% MAs per class
0	113492	(91.82%)	1151	(11.290%)	–	–	–
1	214	(0.17%)	3	(0.037%)	211	19.87%	98.60%
2	2414	(1.95%)	1622	(15.91%)	792	74.58%	32.81%
3	7480	(6.05%)	7421	(72.78%)	59	5.56%	0.78%
TOTAL	78000	(100%)	9942	(100%)	1062	100%	–

4.2 CD Accuracy and Execution Time Results

The results obtained through the application of the CD technique introduced in this paper to the multispectral dataset of Sardinia are detailed in this section. It is worth noting that the changes between the two images of this dataset (See Fig. 2) are not related to the replacement of objects or areas but to the modification of the shapes of relevant objects in the images. The edges between regions are also sharper than for other datasets.

Table 2 shows the accuracies obtained in the binary CD of the Sardinia dataset with different configurations of the binary CD processing. C^2VA is a method based on the computation of distances and angles between the pixel-vectors of the input images where the Euclidean Distance (ED) is used to decide whether a pixel has changed and the angle is used to cluster different types of changes. C^2VA is a technique used in several references in the literature.[5,6] Due to the type of changes present in this dataset, the configuration that achieves the highest accuracy results is the one based on the SAM distance and Otsu's thresholding, without including any additional stage.

The CD maps achieved with the different configurations of the binary CD stage introduced in Table 2 are shown in Fig. 3. A binary CD map corresponding to the C^2VA approach is included for comparison purposes (Fig. 3(a)). It can be seen in Fig. 3 that the maps including spatial information by using the watershed segmentation method (Euclidean+watershed+Otsu and SAM+watershed+Otsu corresponding to Fig. 3(d) and (e)) do not improve the quality of the change detection as compared to the equivalent configurations without considering the spatial information (Fig. 3 (b) and (c)). This is due to the sharp edges among regions present in the dataset, that make the segmentation-based CD technique based on smoothing the segmented regions less effective. Therefore, it is preferable, in this case, to use the configurations without the watershed processing as the computational load of the scheme will be more reduced and the accuracy results slightly better.

For the other configurations (Fig. 3(b-c)), the one based on SAM distance (Fig. 3 (c)) achieves a cleaner CD map, what results in the best accuracy values shown in Table 2. It also detects the change related with the simulated burned area (red area inside the white square in Fig. 2(c)) Nevertheless, the small change related to the enlargement of the open quarry (green area inside the white oval in the bottom right of Fig. 2(c) and class 1 in Table 3) is not detected by the SAM distance. An analysis of the pixels in this area in both images shows that most of the pixels present a similar spectral signature in both images. An example of this is shown in Fig. 4. The SAM distance is invariant to changes of scale, usually related to different illumination conditions. Therefore, it is reasonable that this area is not labeled as change because the spectral signatures of the pixels suggest the presence of the same material in both images of the dataset.

The numerical results of the binary filtering stage for the Sardinia dataset are displayed in Table 3. As explained before, the changes of class 1 (green inside the white oval in Fig. 2(c)), located in the bottom right part of the image, are mostly MAs. The filtering of the changes of class 3, the class including more pixels, correctly passes more than 99% of the changed pixels of the class.

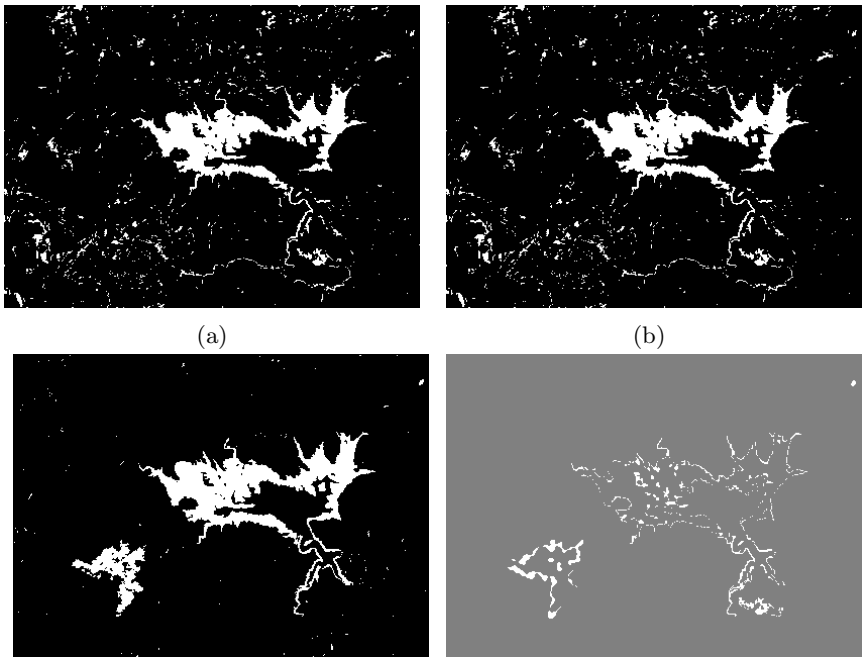

(a) (b) (c) (d)

Figure 3: Sardinia dataset binary CD results. C^{2}VA CD map (a), ED+Otsu CD map (b), SAM+Otsu CD map (c), and hit map for SAM+Otsu {white = miss, gray = hit} (d).

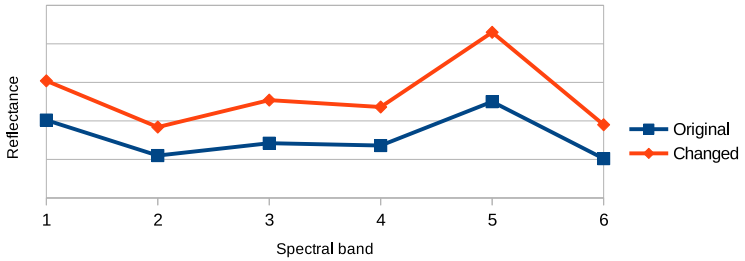

Figure 4: Example of spectral signatures corresponding to a pixel labelled as change of type 1 in the Sardinia dataset.

Finally, Table 4 shows the multiclass CD accuracies for the Sardinia dataset. The difference and stack of the multitemporal information are explored as fusion techniques, and, the resulting bands are also directly passed to the classifiers. The PCA and NWFE FE methods are evaluated retaining 3 components in all the cases. As it can be seen, all the different configurations considered achieve very high accuracies in terms of OA and kappa, above 99.9% and 99.5%, respectively. Nevertheless, in the case of the AA accuracies, it must be taken into account that for one of the three considered classes of change, only 3 pixels remain after the filtering and this is an insufficient number of pixels for an appropriate training and testing of the supervised classifier. So, AA values are low because nearly a full class of change is wrongly classified. Fig. 5 (b) shows the best CD multiclass classification map achieved for the Sardinia dataset. It can be seen in the figure that all the pixels selected as change are classified to the corresponding change class regarding the available reference data. It can also be seen from the table that the FE stage is not critical for the considered dataset, because the original dimensions are small enough. Therefore, the FE techniques are not considered in the remaining experiments presented in this paper.

The execution time required to compute each stage of the proposed CD technique is detailed in Table 5, along with the speedups achieved for the GPU implementation as compared to a 4-thread multicore implementation in CPU using OpenMP. As it can be seen in Table 5, every step involved in both stages of the processing is faster when it is executed in the GPU, achieving a total speedup of 4.2× compared to the OpenMP implementation

Table 4: Multiclass CD accuracies for the Sardinia dataset.

Fusion	FE	SVM					ELM			
		Parameters		OA	AA	k	Parameters	OA	AA	k
		C	γ				N			
		32	1	99.94	66.66	99.80	20	99.95	74.954	99.84
Difference	PCA	32	1	99.92	66.66	99.70	10	99.92	69.91	99.72
	NWFE	32	1	99.93	66.66	99.80	10	99.92	69.90	99.72
		32	1	99.92	**100.00**	99.70	50	**99.97**	91.65	**99.90**
Stack	PCA	32	0.125	99.95	66.66	99.80	10	99.88	76.51	99.57
	NWFE	32	1	**99.97**	**100.00**	**99.90**	10	99.94	76.61	99.79

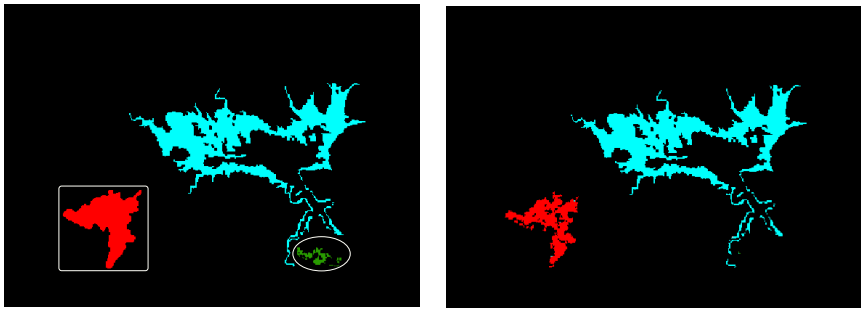

(a) (b)

Figure 5: Reference data of changes (a) and best ELM multiclass CD map (b) for the Sardinia dataset.

Table 5: Multiclass CD execution times (in seconds) for the Sardinia dataset in the presence of noise (AWGN with σ=0.01).

	Binary CD			Multiclass CD				Total
	SAM	Otsu's	Total	Fusion	Filtering	Classification	Total	
OpenMP CPU	0.00622	0.00449	0.01071	0.00166	0.00139	0.05546	0.05851	**0.06922**
CUDA GPU	0.00014	0.00133	0.00147	0.00033	0.00025	0.01434	0.01492	0.01639
Speedup	44.4×	3.4×	7.3×	5.0×	5.6×	3.9×	3.9×	4.2×

used as a baseline. This allows us to execute the entire CD technique in less than 0.07 seconds in GPU. The speedups could be even higher if the dataset considered is large enough to saturate the compute capabilities of the GPU, which is not the case of the Sardinia dataset.

4.3 CD Accuracy Results in the Presence of Noise

The capture of the remote sensing images often results in the appearance of noise in the original spectral signatures. This is the reason why it is important for a remote sensing CD technique to be robust in the presence of noise. In this section, the behavior of the multiclass CD technique in the presence of simulated noise is evaluated. In particular, two types of noise are used to evaluate the robustness of the proposed technique: AWGN and speckle noise. AWGN is a noise model used to resemble the effect of random processes that occur in nature. It is additive because the noise signal is added to the original signal. It has uniform power across the different frequencies, just like the white color is composed of all frequencies in the visible spectrum. The probability distribution of the noise samples is Gaussian. The speckle noise is a granular multiplicative noise as the one present on the capturing process of Synthetic Aperture Radar (SAR) images. This kind of noise comes from random fluctuations in the return signal from an object that is no bigger than a single image-processing element. It increases the mean gray level of a local area.[15]

Different levels of noise are applied to the original spectral signatures by selecting the variance of the noisy signal to be introduced (σ). The Peak Signal-to-Noise Ratio (PSNR) obtained after the application of the noise is used as a measure of the level of degradation of the input images. The PSNR represents the ratio between the maximum possible power of a signal and the power of corrupting noise that affects the fidelity of its

Table 6: Binary CD accuracies for the Sardinia dataset in the presence of noise.

Noise			C^2VA					
Type	σ	**PSNR**	**Correct**		**MAs**	**FAs**	**Total error**	
–	–	–	117990	(95.46%)	2583	3027	5610	(4.54%)
AWGN	0.005	23db	**102335**	**(82.80%)**	1798	**19467**		
	0.01	20db	**84117**	**(68.06%)**	1977	**37506**	**39483**	**(31.94%)**
	0.04	15db	**69964**	**(56.61%)**	4366	**49270**	**53636**	**(43.39%)**
Speckle	005	35db	120085	(97.16%)	2612	**903**	3515	(2.84%)
	0.01	32db	119788	(96.92%)	2620	**1192**	3812	(3.08%)
	0.04	26db	**109161**	**(88.32%)**	2172	**12267**	**14439**	**(11.68%)**
Noise			**SAM+Otsu**					
Type	σ	**PSNR**	**Correct**		**MAs**	**FAs**	**Total error**	
–	–	–	**121387**	**(98.21%)**	**1062**	**1151**	**2213**	**(1.79%)**
AWGN	0.005	23db	91446	(73.99%)	**988**	31166	32154	(26.01%)
	0.01	20db	73841	(59.74%)	**1063**	48696	49759	(40.26%)
	0.04	15db	69159	(55.95%)	**2884**	51557	54441	(44.05%)
Speckle	005	35db	**121282**	**(98.12%)**	**1349**	969	**2318**	**(1.88%)**
	0.01	32db	**121001**	**(97.90%)**	**1261**	1338	**2599**	**(2.10%)**
	0.04	26db	107901	(87.30%)	**1099**	14600	15699	(12.70%)

representation. It is expressed in terms of decibels (db), in a logarithmic scale, to deal with the wide dynamic range present in many signals.

The effects of different levels of AWGN and speckle noise in the first stage of the technique, the binary CD classification, are shown in Tables 6 and 7. Table 6 shows the results of the binary stage of the CD in terms of correctly classified pixels, MA, FA, and total error. Table 7 details the accuracies achieved for the change and no change classes. Three different variance levels (σ) were considered for each type of noise, being the input images scaled in the range $[0-1]$. The PSNR obtained after the application of each considered noise is also shown in the tables as a measure of the level of degradation of the input images.

Table 6 shows the binary results for the SAM+Otsu binary approach proposed in this paper and also for C^2VA. It can be seen that for both techniques and both types of noise, the higher the degradation of the signal the lower the CD accuracies obtained. In terms of total correctly classified pixels, the C^2VA outperforms the SAM+Otsu technique for the three levels of AWGN noise and the larger level of speckle noise. Nevertheless, a careful analysis shows that the SAM+Otsu technique achieves lower MAs values in the six considered scenarios. This is important because the MAs values are directly related to the amount of changes that the technique is unable to detect.

Table 7 shows in detail the results of Table 6, expressed as percentages, for the change and no change classes. As it can be checked in the table, the proposed SAM+Otsu technique maintains a better accuracy in the change pixels in the six scenarios. In fact, in five of the six noise cases considered, the proposed technique maintains an accuracy for the pixels of the change class similar to the one achieved in the dataset without noise. The accuracy for the change class only decreases drastically in the case of AWGN noise with σ=0.04 where the PSNR is only 15 decibels.

Regarding the multiclass accuracies, i.e., the final results of the CD scheme, that are calculated over the pixels selected as change by the binary stage, can be seen in Table 8. The proposed multiclass CD technique achieves better results in the presence of noise than the C^2VA in five of the six noise scenarios considered. The proposed technique performs better, independently of the fusion method (difference or stack of the input images) and the classification algorithm considered (SVM or ELM). The C^2VA achieves a slightly better result in the case of AWGN with σ=0.04 but it must be taken into account that for this scenario only 57% of the change pixels were correctly filtered in the binary stage.

Table 7: Detailed per class binary CD accuracies, as percentages, for the Sardinia dataset in the presence of noise.

Noise			C^2VA		SAM+Otsu	
Type	σ	**PSNR**	**Change**	**No change**	**Change**	**No change**
–	–	–	74.45	97.33	**89.49**	**98.99**
	0.005	23db	82.21	**82.84**	**90.22**	72.54
AWGN	0.01	20db	80.44	**66.95**	**89.48**	57.09
	0.04	15db	56.81	**56.58**	**71.47**	54.57
	0.005	35db	74.16	**99.20**	**86.65**	99.15
Speckle	0.01	32db	74.08	**98.94**	**87.52**	98.82
	0.04	26db	78.51	**89.19**	**89.13**	87.14

Table 8: Multiclass CD accuracies in terms of OA for the Sardinia dataset in the presence of noise.

Noise			C^2VA	Difference		Stack	
Type	σ	**PSNR**		**SVM**	**ELM**	**SVM**	**ELM**
–	–	–	99.30	99.94	99.95	99.92	**99.97**
	0.005	23db	93.56	97.13	97.19	97.91	**98.05**
AWGN	0.01	20db	91.17	94.65	94.17	**95.83**	95.28
	0.04	15db	**86.45**	85.53	86.02	86.12	86.41
	0.005	35db	99.20	99.92	99.93	**99.98**	99.96
Speckle	0.01	32db	98.89	99.91	99.92	99.93	**99.94**
	0.04	26db	96.81	99.74	99.77	**99.90**	99.88

From this analysis, it can be extracted that the proposed CD scheme is sensitive to noisy conditions, especially, in the binary stage of the CD. Therefore, the introduction of denoising techniques before the first stage of the CD technique should be considered to achieve a more robust multiclass CD for multitemporal images.

5. CONCLUSIONS

A multiclass CD technique for multitemporal multidimensional images that is robust in noisy conditions was presented in this paper. The proposed CD combines binary and multiclass stages in order to obtain a detailed change classification map including *from-to* transition information. The combination of the binary CD stage with the multiclass one, also allows to obtain a more efficient CD scheme, reducing the computational cost of the multiclass stage of the technique. Furthermore, the GPU projection of the proposed technique allows us to compute it efficiently in commodity hardware.

The proposed technique was evaluated in a multispectral dataset from the literature, showing its suitability to be used in multidimensional images. The binary stage of the CD achieves 98.21% of correctly detected changes while the multiclass stage correctly classifies to the right transition up to 99.97% of the changes detected. The behavior of the proposed CD was tested in the presence of different types (AWGN and speckle) and magnitudes of noise in the input dataset. The proposed technique maintains accuracies that are very similar to those achieved without noise in all the scenarios considered, being more robust than the C^2VA alternative from the literature.

Regarding the execution times, the CD technique is computed in less than 0.02 seconds in GPU for the Sardinia dataset used in this paper, being 4.5× faster than an optimized OpenMP version of the same technique. Speedups up to 44.4× are achieved in some stages of the processing.

ACKNOWLEDGMENTS

This work was supported in part by the Consellería de Cultura, Educación e Ordenación Universitaria [grant numbers GRC2014/008 and ED431G/08] and the Ministry of Education, Culture and Sport, Government of Spain [grant number TIN2016-76373-P] both are co–funded by the European Regional Development Fund (ERDF). This work was also partially supported by Junta de Castilla y León - ERDF (PROPHET Project) [grant number VA082P17].

REFERENCES

[1] Singh, A., "Review article digital change detection techniques using remotely-sensed data," *International Journal of Remote Sensing* **10**(6), 989–1003 (1989).

[2] Bovolo, F. and Bruzzone, L., "The time variable in data fusion: A change detection perspective," *Geoscience and Remote Sensing Magazine, IEEE* **3**(3), 8–26 (2015).

[3] Bannari, A., Morin, D., Bonn, F., and Huete, A., "A review of vegetation indices," *Remote sensing reviews* **13**(1-2), 95–120 (1995).

[4] Malila, W. A., "Change vector analysis: an approach for detecting forest changes with Landsat," in [*LARS Symposia*], 385 (1980).

[5] Liu, S., Bruzzone, L., Bovolo, F., Zanetti, M., and Du, P., "Sequential spectral change vector analysis for iteratively discovering and detecting multiple changes in hyperspectral images," *Geoscience and Remote Sensing, IEEE Transactions on* **53**(8), 4363–4378 (2015).

[6] Liu, S., Du, Q., Tong, X., Samat, A., Bruzzone, L., and Bovolo, F., "Multiscale morphological compressed change vector analysis for unsupervised multiple change detection," *IEEE Journal of Selected Topics in Applied Earth Observations and Remote Sensing* **10**(9), 4124–4137 (2017).

[7] Ghosh, A., Subudhi, B. N., and Bruzzone, L., "Integration of gibbs markov random field and hopfield-type neural networks for unsupervised change detection in remotely sensed multitemporal images," *Image Processing, IEEE Transactions on* **22**(8), 3087–3096 (2013).

[8] Hao, M., Shi, W., Zhang, H., and Li, C., "Unsupervised change detection with expectation-maximization-based level set," *Geoscience and Remote Sensing Letters, IEEE* **11**(1), 210–214 (2014).

[9] Volpi, M., Tuia, D., Bovolo, F., Kanevski, M., and Bruzzone, L., "Supervised change detection in VHR images using contextual information and support vector machines," *International Journal of Applied Earth Observation and Geoinformation* **20**, 77–85 (2013).

[10] Kempeneers, P., Sedano, F., Strobl, P., McInerney, D. O., and San-Miguel-Ayanz, J., "Increasing robustness of postclassification change detection using time series of land cover maps," *Geoscience and Remote Sensing, IEEE Transactions on* **50**(9), 3327–3339 (2012).

[11] Benediktsson, J. A., Pesaresi, M., and Amason, K., "Classification and feature extraction for remote sensing images from urban areas based on morphological transformations," *IEEE Transactions on Geoscience and Remote Sensing* **41**(9), 1940–1949 (2003).

[12] Celik, T., "Unsupervised change detection in satellite images using principal component analysis and K-means clustering," *Geoscience and Remote Sensing Letters, IEEE* **6**(4), 772–776 (2009).

[13] Kuo, B.-C. and Landgrebe, D. A., "A robust classification procedure based on mixture classifiers and nonparametric weighted feature extraction," *IEEE Transactions on Geoscience and Remote Sensing* **40**(11), 2486–2494 (2002).

[14] Radke, R. J., Andra, S., Al-Kofahi, O., and Roysam, B., "Image change detection algorithms: a systematic survey," *IEEE transactions on image processing* **14**(3), 294–307 (2005).

[15] Tso, B. and Mather, P. M., [*Classification methods for remotely sensed data*], no. LC-0431, CRC press (2009).

[16] Plaza, A., Du, Q., Chang, Y.-L., and King, R. L., "High performance computing for hyperspectral remote sensing," *IEEE Journal of Selected topics in applied earth observations and remote sensing* **4**(3), 528–544 (2011).

[17] Christophe, E., Michel, J., and Inglada, J., "Remote sensing processing: From multicore to GPU," *IEEE Journal of Selected Topics in Applied Earth Observations and Remote Sensing* **4**(3), 643–652 (2011).

[18] Yang, B., Yang, M., Plaza, A., Gao, L., and Zhang, B., "Dual-mode FPGA implementation of target and anomaly detection algorithms for real-time hyperspectral imaging," *IEEE Journal of Selected Topics in Applied Earth Observations and Remote Sensing* **8**(6), 2950–2961 (2015).

[19] Zhang, W., Luo, G., Shen, L., Page, T., Li, P., Jiang, M., Maass, P., and Cong, J., "FPGA acceleration by asynchronous parallelization for simultaneous image reconstruction and segmentation based on the mumford-shah regularization," in [*SPIE Optical Engineering+ Applications*], 96000H–96000H, International Society for Optics and Photonics (2015).

[20] Quesada-Barriuso, P., Argüello, F., and B. Heras, D., "Computing efficiently spectral-spatial classification of hyperspectral images on commodity GPUs," in [*Recent Advances in Knowledge-Based Paradigms and Applications*], 19–42, Springer (2014).

[21] López-Fandiño, J., Quesada-Barriuso, P., B. Heras, D., and Argüello, F., "Efficient ELM-based techniques for the classification of hyperspectral remote sensing images on commodity GPUs," *IEEE Journal of Selected topics in applied earth observations and remote sensing* **8**(6), 2884 – 2893 (2015). DOI:10.1109/JSTARS.2014.2384133.

[22] Sánchez, S., Ramalho, R., Sousa, L., and Plaza, A., "Real-time implementation of remotely sensed hyperspectral image unmixing on GPUs," *Journal of Real-Time Image Processing* **10**(3), 469–483 (2015).

[23] Chen, Z., Vatsavai, R. R., Ramachandra, B., Zhang, Q., Singh, N., and Sukumar, S., "Scalable nearest neighbor based hierarchical change detection framework for crop monitoring," in [*Big Data (Big Data), 2016 IEEE International Conference on*], 1309–1314, IEEE (2016).

[24] Zhu, H., Cao, Y., Zhou, Z., and Gong, M., "Parallel multi-temporal remote sensing image change detection on GPU," in [*Parallel and Distributed Processing Symposium Workshops & PhD Forum (IPDPSW), 2012 IEEE 26th International*], 1898–1904, IEEE (2012).

[25] López-Fandiño, J., Priego, B., B. Heras, D., Argüello, F., and J. Duro, R., "GPU projection of ECAS-II segmenter for hyperspectral images based on cellular automata," *IEEE Journal of Selected Topics in Applied Earth Observations and Remote Sensing* **10**(1), 20–28 (2017). DOI:10.1109/JSTARS.2016.2588530.

[26] Plaza, A., Benediktsson, J. A., Boardman, J. W., Brazile, J., Bruzzone, L., Camps-Valls, G., Chanussot, J., Fauvel, M., Gamba, P., Gualtieri, A., et al., "Recent advances in techniques for hyperspectral image processing," *Remote Sensing of Environment* **113**, S110–S122 (2009).

[27] Zhao, W. and Du, S., "Spectral–spatial feature extraction for hyperspectral image classification: A dimension reduction and deep learning approach," *IEEE Transactions on Geoscience and Remote Sensing* **54**(8), 4544–4554 (2016).

[28] Nvidia, *NVIDIA Tesla P100 The Most Advanced Data Center Accelerator Ever Built. Featuring Pascal P100, the Worlds Fastest GPU* (2016).

[29] Nvidia, *CUBLAS Library User Guide* (2013).

[30] Tomov, S., Nath, R., Du, P., and Dongarra, J., "MAGMA users guide," *ICL, UTK (November 2009)* (2011).

[31] Nvidia, "Cula tools," Available at: http://www.culatools.com/ (Accessed Februrary 2018).

[32] Survey, U. S. G., "Thematic mapper sensor website," (Accessed Februrary 2018). Available at: https://lta.cr.usgs.gov/TM.

[33] Bovolo, F., Marchesi, S., and Bruzzone, L., "A framework for automatic and unsupervised detection of multiple changes in multitemporal images," *IEEE Transactions on Geoscience and Remote Sensing* **50**(6), 2196–2212 (2012).

[34] Demir, B., Bovolo, F., and Bruzzone, L., "Detection of land-cover transitions in multitemporal remote sensing images with active-learning-based compound classification," *Geoscience and Remote Sensing, IEEE Transactions on* **50**(5), 1930–1941 (2012).

[35] Bruzzone, L. and Prieto, D. F., "Automatic analysis of the difference image for unsupervised change detection," *Geoscience and Remote Sensing, IEEE Transactions on* **38**(3), 1171–1182 (2000).